Circularly Polarized Thermal Radiation From Nonequilibrium Coupled Antennas

Chinmay Khandekar* and Zubin Jacob
Birck Nanotechnology Center, School of Electrical and Computer Engineering, College of Engineering, Purdue University, West Lafayette, Indiana 47907, USA

(Received 6 December 2018; revised manuscript received 10 June 2019; published 26 July 2019)

Circularly polarized light can be obtained by using either polarization conversion or structural chirality. Here we reveal a fundamentally unrelated mechanism of generating circularly polarized light using coupled nonequilibrium sources. We show that thermal emission from a compact dimer of subwavelength, anisotropic antennas can be highly circularly polarized when the antennas are at unequal temperatures. Furthermore, the handedness of emitted light is flipped upon interchanging the temperatures of the antennas, thereby enabling reconfigurability of the polarization state lacked by most circularly polarized light sources. We describe the fundamental origin of this mechanism using rigorous fluctuational electrodynamic analysis and further provide practical examples for its experimental implementation. Apart from the technology applications in reconfigurable devices, communication, and sensing, this work motivates new inquiries of angular-momentum-related thermal-radiation phenomena using thermal nonequilibrium, without applying magnetic field.

DOI: 10.1103/PhysRevApplied.12.014053

I. INTRODUCTION

Circularly polarized (CP) light has recently acquired great attention in the context of spin-controlled nanophotonics [1,2], spintronics [3], and chiral quantum optics [4], where its spin angular momentum is harnessed for engineering spin-dependent light-matter interactions at nanoscale. Given its fundamental and technological importance, there is a strong demand for CP-light sources having high purity and compactness with and without reconfigurability of the polarization state.

One approach to obtain CP light is by passing unpolarized light through a linear polarizer followed by an optimized polarization conversion device such as a metasurface [5–7], which can preferentially convert it into right circularly polarized (RCP) light or left circularly polarized (LCP) light. Another more fundamental approach utilizes structural (geometric and material) chirality at the level of the source, examples of which include a long list of electroluminescent [8–12] and photoluminescent [13–16] CP-light sources. Apart from these approaches, CP-light generation via thermal radiation (incandescence) has been demonstrated experimentally using the same underlying mechanisms [17,18]. These are a few representative examples of all types of CP-light sources, which are fundamentally based on either polarization conversion or structural chirality.

In this work, we demonstrate a different mechanism of generating CP light based on near-field coupling between nonequilibrium sources. It is unrelated to polarization conversion or chirality and cannot be described using those concepts. This mechanism is useful because practically, it solves the challenging problem of reconfigurability of the polarization state lacked by most CP-light sources. Fundamentally, it reveals an unforeseen connection between thermal nonequilibrium and angular momentum of light.

We consider a dimer system of two perpendicularly oriented, subwavelength, anisotropic shaped antennas depicted in Fig. 1. We analyze the spin angular momentum of thermal emission from the dimer using fluctuational electrodynamics. We note that this approach [19] remains largely unexplored in the field of thermal radiation despite many decades of separate works on radiative heat transfer [20,21] and angular momentum of nonthermal light [22,23]. The fluctuational electrodynamic analysis reveals that suitable correlations (imaginary valued) between orthogonal components of thermally fluctuating sources are necessary for emission of CP light. We find that the strong correlations are realized through near-field interactions between the antennas when they are held at unequal temperatures (nonequilibrium). On the other hand, antennas at equal temperatures emit very weakly polarized thermal radiation. Interestingly, for nonequilibrium antennas, the handedness of emitted radiation is flipped upon interchanging the temperatures of the antennas thus enabling reconfigurability of the polarization state lacked

*ckhandek@purdue.edu

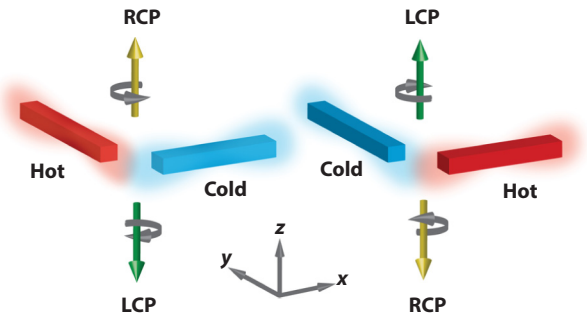

FIG. 1. A pair of anisotropic shaped, subwavelength (dipolar), coupled antennas at unequal temperatures can emit strongly circularly polarized light in suitable directions (upper and lower hemispheres). Handedness and directionality of emitted polarized radiation is switched upon interchanging the temperatures of two antennas.

by most CP-light sources [17,18]. We further explore the experimental feasibility of observing this phenomenon with dimers of antennas made of silicon carbide (SiC) and indium phosphide (InP), amongst many other plasmonic and polaritonic materials. The resonantly enhanced near-field interaction between the localized dipolar modes of the antennas, leads to reasonably strong midinfrared CP-light emission under a temperature difference of $\Delta T \sim 30$ K across a separation of $d \sim 1\,\mu$m between the antennas. This should be experimentally realizable in the near future since a significant experimental progress in measuring near-field radiative heat transfer has facilitated exploration of large temperature differences at nanoscale and has verified the validity of fluctuational electrodynamic theory [24–26]. We further provide another conceptual example system based on plasmonic nanolaser, operated well below lasing threshold, where amplified spontaneous emission is described using fluctuational electrodynamics. That example demonstrates that the proposed mechanism is not limited to "thermal" nonequilibrium but can also be implemented in other forms such as population inversion of gain atoms, paving the way for CP-light-emitting LEDs.

In comparison to other solid-state designs that can emit CP thermal radiation [17,18,27,28], the proposed mechanism offers a practical advantage of temperature-based polarization reconfigurability. The underlying fluctuational electrodynamic analysis sheds additional light on previous designs and expands the design space by incorporating nonequilibrium systems. In the field of thermal radiation, the proposed mechanism reveals a nonintuitive fundamental connection between thermal nonequilibrium and angular momentum of light. While almost all studies of angular momentum of light are primarily limited to nonthermal light [29–31], few recent studies [19,32] have started to explore related thermal-radiation phenomena. But they require application of magnetic field. Our work suggests the possibility of exploring such phenomena using thermal nonequilibrium without applying magnetic field. In the context of using nonequilibrium systems for shaping thermal radiation, other recent works have explored directional emissivity [33,34], nontrivial thermal forces and torques [35], and enhanced emissivity from nonequilibrium antennas [36]. Our work conveys that one can take advantage of temperature-based reconfigurability in nonequilibrium systems, for numerous applications in communications, sensing, and detection technologies.

We divide the paper into the following parts. In Sec. II, we demonstrate circular polarization (spin angular momentum) of thermal emission from the dimer system of Fig. 1 using fluctuational electrodynamics. We describe the fundamental origin of CP-light emission from nonequilibrium antennas and further provide general design guidelines for systems more complicated than the proposed dimer. In Sec. III, we explore the practical implementation of the proposed mechanism by considering realistic SiC and InP antenna dimers and a conceptual plasmonic nanolaser system as another viable option. Finally, we conclude by highlighting the fundamental and technological relevance of this work and future research directions in Sec. IV.

II. DIMER OF ANTENNAS

Theory: Thermal radiation consists of electromagnetic fields generated by thermal, stochastic motion of charges. These can be calculated from Maxwell's equations by introducing fluctuating currents provided they satisfy specific fluctuation-dissipation relations [20,37]. To study thermal emission from a dimer of subwavelength antennas, we consider one variant of this fluctuational electrodynamic approach termed as the finite dipole model, where thermal sources are randomly fluctuating dipole moments of dipolar sources, satisfying specific fluctuation-dissipation relations [38–40]. We consider the geometry depicted in Fig. 1 consisting of two subwavelength (dipolar), anisotropic antennas placed near the origin in vacuum with their long axes oriented along arbitrary $\hat{\mathbf{e}}_1$ and $\hat{\mathbf{e}}_2$ directions. The antennas have temperatures T_1, T_2 and vacuum polarizabilities α_1, α_2 along their orientations, respectively. The fluctuating dipole moments of these dipolar antennas in the absence of any interactions are given by $p_1\hat{\mathbf{e}}_1$ and $p_2\hat{\mathbf{e}}_2$ which satisfy the following fluctuation-dissipation relations in the frequency domain [38–40]:

$$\langle p_j^*(\omega)p_k(\omega')\rangle = \frac{2\varepsilon_0}{\omega}\mathrm{Im}\{\alpha_j\}\Theta(\omega, T_j)\delta(\omega-\omega')\delta_{jk}. \quad (1)$$

Here $\{j,k\} = \{1,2\}$, $\Theta(\omega,T) = \hbar\omega/2 + \hbar\omega/[\exp(\hbar\omega/k_BT) - 1]$ is the mean thermal energy of a Harmonic oscillator of frequency ω. T_j is the temperature of dipolar object and $\langle\cdots\rangle$ denotes statistical ensemble average. When the dipoles are placed close to each other, the interactions

between them lead to effective dipole moments:

$$\tilde{p}_j = p_j + \varepsilon_0 \alpha_j [\mathbf{E}_{jk}(\tilde{p}_k) \cdot \hat{\mathbf{e}}_j] \tag{2}$$

for $j \neq k$. $\mathbf{E}_{jk}(\tilde{p}_k)$ denotes the electric field at dipole j due to dipole k. It is straightforward to calculate the far-field thermal radiation as well as the near-field-induced correlations of the effective dipole moments using the general expressions,

$$\mathbf{E}(\omega) = \frac{k_0^3}{4\pi\varepsilon_0}\frac{e^{ik_0R}}{(k_0R)}\left\{[\hat{\mathbf{e}}_j - (\hat{\mathbf{e}}_j \cdot \hat{\mathbf{e}}_R)\hat{\mathbf{e}}_R] + \frac{ik_0R-1}{(k_0R)^2}[\hat{\mathbf{e}}_j - 3(\hat{\mathbf{e}}_j \cdot \hat{\mathbf{e}}_R)\hat{\mathbf{e}}_R]\right\}\tilde{p}_j, \tag{3}$$

$$\mathbf{H}(\omega) = \frac{k_0^3}{4\pi\varepsilon_0}\frac{e^{ik_0R}}{(k_0R)}\sqrt{\frac{\varepsilon_0}{\mu_0}}\left[1 + \frac{i}{k_0R}\right](\hat{\mathbf{e}}_R \times \hat{\mathbf{e}}_j)\tilde{p}_j \tag{4}$$

for the electromagnetic fields at a point $R\hat{\mathbf{e}}_R$ due to a single dipole $\tilde{p}_j\hat{\mathbf{e}}_j$ at the origin with $k_0 = \omega/c$ being the vacuum wavevector.

The intensity flux of thermal radiation is given by the Poynting vector in the far field ($\mathrm{Re}\{\mathbf{E}^*(\omega) \times \mathbf{H}(\omega)\}$) and the degree of circular polarization is measured by the spin-angular-momentum density of thermal emission. By generalizing the definitions employed for nonthermal light in several works [22,30,41] to thermal radiation [19], we write the spectral energy density $\langle W(\omega)\rangle$ and spin-angular-momentum density $\langle \mathbf{S}(\omega)\rangle$ of emitted light in vacuum as

$$\langle W(\omega)\rangle = \frac{1}{2}\langle \varepsilon_0 \mathbf{E}^*(\omega) \cdot \mathbf{E}(\omega) + \mu_0 \mathbf{H}^*(\omega) \cdot \mathbf{H}(\omega)\rangle, \tag{5}$$

$$\langle \mathbf{S}(\omega)\rangle = \frac{1}{2\omega}\mathrm{Im}\{\langle \varepsilon_0 \mathbf{E}^*(\omega) \times \mathbf{E}(\omega) + \mu_0 \mathbf{H}^*(\omega) \times \mathbf{H}(\omega)\rangle\}. \tag{6}$$

Note the use of $\langle \cdots \rangle$, which denotes the statistical ensemble average of physical quantities in the context of thermally generated radiation. We further define a dimensionless vector quantity called the spectral thermal spin,

$$\mathbf{S}_T(\omega) = \frac{\omega\langle \mathbf{S}(\omega)\rangle}{\langle W(\omega)\rangle}, \tag{7}$$

whose magnitude in a given direction lies between $[-1, 1]$ with -1 denoting pure LCP light and $+1$ denoting pure RCP light along that direction. In an actual experiment, this direction can be along the axis of a detector. Since the quantity given by Eq. (6) remains largely unexplored in the field of thermal radiation and may not be familiar to researchers working on thermal radiation and heat-transfer topics, we point out its connection with closely related well-known concepts. In particular, one can also understand the spin of thermal radiation in the more familiar language of Stokes polarimetry. The Stokes S_3 parameter describes the circular polarization of the fields lying transverse to a given propagation direction. If one calculates the Stokes S_3 parameters for thermally generated fields in all three orthogonal coordinate planes [42], one retrieves a form similar to Eq. (6). It is also well known that circularly polarized laser light can impart angular momentum to small, absorptive particles in its path causing them to rotate about their own axis [43]. It is then meaningful to calculate the spin angular momentum of light [Eq. (6)] since optical torque on these particles is proportionate to it [44,45].

We calculate the spectral thermal spin given by Eq. (7) for the example geometry of two dipolar antennas placed close to each other near the origin with their centers at $\mathbf{x}_1$ and $\mathbf{x}_2 = \mathbf{x}_1 + d\hat{\mathbf{e}}_d$. The fluctuating dipole moments and associated correlations such as $\langle \tilde{p}_j^*(\omega)\tilde{p}_k(\omega)\rangle$ are calculated using Eqs. (1)–(4). The calculation of electromagnetic fields and other related quantities in the far field at a point $R\hat{\mathbf{e}}_R$ is simplified since only the leading-order terms $\mathcal{O}(1/k_0R)$ are important. The distances between dipoles and $R\hat{\mathbf{e}}_R$ in the far field are $R_j = |R\hat{\mathbf{e}}_R - \mathbf{x}_j| = R - \mathbf{x}\cdot\hat{\mathbf{e}}_R$. Using simple algebraic manipulations, we derive the following expression for the spectral thermal spin in the far field at a point $R\hat{\mathbf{e}}_R$:

$$\mathbf{S}_T(\omega) = \frac{2\mathrm{Im}\{e^{ik_0(\mathbf{x}_1-\mathbf{x}_2)\cdot\hat{\mathbf{e}}_R}\langle \tilde{p}_1^*(\omega)\tilde{p}_2(\omega)\rangle\}[(\hat{\mathbf{e}}_1 \times \hat{\mathbf{e}}_2)\cdot\hat{\mathbf{e}}_R]\hat{\mathbf{e}}_R}{\sum_{j,k=1,2} e^{ik_0(\mathbf{x}_j-\mathbf{x}_k)\cdot\hat{\mathbf{e}}_R}\langle \tilde{p}_j^*(\omega)\tilde{p}_k(\omega)\rangle[(\hat{\mathbf{e}}_j\cdot\hat{\mathbf{e}}_k) - (\hat{\mathbf{e}}_j\cdot\hat{\mathbf{e}}_R)(\hat{\mathbf{e}}_k\cdot\hat{\mathbf{e}}_R)]},$$

$$\langle \tilde{p}_1^*(\omega)\tilde{p}_2(\omega)\rangle = \frac{2\varepsilon_0}{\omega|D|^2}[(\alpha_2 k_0^3\kappa)\mathrm{Im}\{\alpha_1\}\Theta(\omega, T_1) + (\alpha_1 k_0^3\kappa)^*\mathrm{Im}\{\alpha_2\}\Theta(\omega, T_2)], \quad D = 1 - \alpha_1\alpha_2 k_0^6\kappa^2, \tag{8}$$

$$\langle |\tilde{p}_1(\omega)|^2\rangle = \frac{2\varepsilon_0}{\omega|D|^2}[\mathrm{Im}\{\alpha_1\}\Theta(\omega, T_1) + \mathrm{Im}\{\alpha_2\}\Theta(\omega, T_2)|\alpha_1 k_0^3\kappa|^2], \quad \langle |\tilde{p}_2(\omega)|^2\rangle = \langle |\tilde{p}_1(\omega)|^2\rangle(1 \leftrightarrow 2).$$

The dimensionless near-field coupling κ between the two dipoles is given by

$$\kappa = \frac{e^{ik_0d}}{4\pi(k_0d)^3}\left\{(k_0d)^2[(\hat{\mathbf{e}}_1\cdot\hat{\mathbf{e}}_2) - (\hat{\mathbf{e}}_1\cdot\hat{\mathbf{e}}_d)(\hat{\mathbf{e}}_2\cdot\hat{\mathbf{e}}_d)] + (ik_0d - 1)[(\hat{\mathbf{e}}_1\cdot\hat{\mathbf{e}}_2) - 3(\hat{\mathbf{e}}_1\cdot\hat{\mathbf{e}}_d)(\hat{\mathbf{e}}_2\cdot\hat{\mathbf{e}}_d)]\right\}.$$

Equation (8) is the central result of this work, which offers many analytic insights regarding generation of CP light as discussed below.

Necessary condition for emission of CP light: It follows from Eq. (8) that the spin of far-field thermal emission is always radial, which we identify as radial thermal spin $S_R = \mathbf{S}_T \cdot \hat{\mathbf{e}}_R$. Evidently $S_R = 0$ in all directions ($\hat{\mathbf{e}}_R$) when $\hat{\mathbf{e}}_1 = \hat{\mathbf{e}}_2$ (parallel dipoles) and $\mathrm{Im}\{e^{ik_0(\mathbf{x}_1-\mathbf{x}_2)\cdot\hat{\mathbf{e}}_R}\langle\tilde{p}_1^*(\omega)\tilde{p}_2(\omega)\rangle\} = 0$ (no correlations). The latter condition can be used to find the necessary condition for emission of CP radiation from an arbitrary body. We note that if instead of two physically separate antennas, a single dipolar object with dipole moments $p_j\hat{\mathbf{e}}_j$ for $j \in [x, y, z]$ is considered, then it follows that the correlations $\mathrm{Im}\{\langle\tilde{p}_j^*(\omega)\tilde{p}_k(\omega)\rangle\}$ between these orthogonal components are necessary to produce CP radiation in the far field. Since it is not possible to have nonzero thermal spin with zero correlations between orthogonal components of underlying fluctuating sources, it follows that this is a necessary condition for generation of CP light. This condition can be generalized to arbitrary bodies by discretizing them into subvolumes much smaller than the emission wavelength and conceptualized as electric point dipoles. This approach is known as thermal discrete dipole approximation [46,47]. It follows that the correlations $\mathrm{Im}\{\langle\tilde{p}_j^*(\omega)\tilde{p}_k(\omega)\rangle\}$ between the orthogonal components of the effective dipole moments of these subvolumes are necessary to emit CP light.

This finding that the imaginary-valued correlations are necessary for emission of CP light is also an important result of this work. It is insightful for designing CP thermal light sources. For instance, the environment surrounding a dipolar thermal emitter can be engineered such that the imaginary-valued correlations between the effective dipole-moment components are nonzero and consequently, light emitted is circularly polarized. We note that, for arbitrary bodies of nondipolar nature, the necessary condition may not be sufficient since there can be cancellation of spin due to contribution from dipoles of many tiny subvolumes, requiring a full calculation to infer the circular polarization of total radiation emitted by such a body. Nonetheless, such calculations could be performed with advanced computational tools [47,48] and using definition (6) above. In this work, we first focus on a simple dipolar dimer, which is easier to understand, analyze, and optimize.

Optimum design for maximum purity CP light along normal direction: We now find a design that emits maximum purity ($S_R = \pm 1$) CP thermal radiation. To simplify the optimization, we consider the example geometry of Fig. 1 with $\hat{\mathbf{e}}_1 = \hat{\mathbf{e}}_x$, $\hat{\mathbf{e}}_2 = \hat{\mathbf{e}}_y$ (antennas lying in the x-y plane) and focus on thermal emission in $\hat{\mathbf{e}}_z$ direction. Since the phase factor $e^{ik_0(\mathbf{x}_1-\mathbf{x}_2)\cdot\hat{\mathbf{e}}_z} = 1$ for $\hat{\mathbf{e}}_z$ direction, radial spin $S_R \sim \mathrm{Im}\{\langle\tilde{p}_1^*(\omega)\tilde{p}_2(\omega)\rangle\}$ and useful analytical expressions can be obtained. Considering a practically relevant situation of equal vacuum polarizabilities $\alpha_1 = \alpha_2 = \alpha$, one finds that the radial thermal spin $S_R \sim \mathrm{Im}[\alpha k_0^3\kappa + (\alpha k_0^3\kappa)^*\Theta(\omega, T_2)/\Theta(\omega, T_1)]$. This yields $S_R = 0$ when both the dipolar antennas are at equal temperatures $T_1 = T_2$. Therefore, we consider nonequilibrium configuration ($T_1 \neq T_2$) for which the radial thermal spin in the (normal) direction $\hat{\mathbf{e}}_R = \hat{\mathbf{e}}_z$ is

$$S_R = \frac{2\mathrm{Im}\left\{\tilde{\alpha} + \tilde{\alpha}^*\frac{\Theta(\omega,T_2)}{\Theta(\omega,T_1)}\right\}}{(1+|\tilde{\alpha}|^2)\left\{1+\frac{\Theta(\omega,T_2)}{\Theta(\omega,T_1)}\right\} - 2\mathrm{Re}\left\{\tilde{\alpha} + \tilde{\alpha}^*\frac{\Theta(\omega,T_2)}{\Theta(\omega,T_1)}\right\}}.$$

Here, the dimensionless, normalized polarizability $\tilde{\alpha} = \alpha k_0^3\kappa$ is introduced to capture the dependence of radial spin S_R on material properties (polarizability α), geometry (near-field coupling κ) and wavelength and wavevector (k_0) in a concise manner. It follows that when the normalized polarizability $\tilde{\alpha} = \pm i$, $S_R = \pm[\Theta(\omega, T_1) - \Theta(\omega, T_2)]/[\Theta(\omega, T_1) + \Theta(\omega, T_2)]$. This gives high-purity circular polarization ($S_R \to \pm 1$) when the ratio $\Theta(\omega, T_2)/\Theta(\omega, T_1)$ is either very large or very small. We illustrate with practical examples further below that this dependence on both wavelength and temperature makes strong CP light feasible even when temperatures T_1, T_2 are not very different. In the following, not restricting ourselves to $\hat{\mathbf{e}}_z$ direction, we explore the dependence of handedness on various design parameters.

Dependence on antenna temperatures: For small separation between the antennas ($k_0 d < 1$), it follows from Eq. (8) that $S_R \propto \mathrm{Im}\{\langle\tilde{p}_1^*(\omega)\tilde{p}_2(\omega)\rangle\}$. Under this condition, for any geometric configuration of two nonequilibrium coupled antennas of equal polarizabilities ($\alpha_1 = \alpha_2$), the thermal spin is flipped ($S_R \to -S_R$) upon interchanging the temperatures of the antennas. While there is no specific advantage of using antennas of unequal polarizabilities ($\alpha_1 \neq \alpha_2$), similar flipping of handedness (sign of S_R) is observed but the change in the magnitude of S_R depends on the polarizabilities. As we show further below, it is difficult to realize high-purity ($|S_R| \sim 1$) CP radiation at large separations due to decreased near-field interactions. But similar tunability of handedness based on temperatures is observed at large separations for weakly polarized light.

Dependence on emission direction: We note that only one of the normalized polarizability conditions $\alpha k_0^3\kappa = \pm i$ is true depending on the sign of near-field coupling κ since the condition $\mathrm{Im}\{\alpha\} > 0$ must hold true for real, passive (lossy) dipoles [49]. For the example configuration with horizontal ($\hat{\mathbf{e}}_x$) and vertical ($\hat{\mathbf{e}}_y$) dipoles with relative orientation $\hat{\mathbf{e}}_d = (-\hat{\mathbf{e}}_x + \hat{\mathbf{e}}_y)/\sqrt{2}$, the coupling $\kappa = e^{ik_0 d}/8\pi(k_0 d)^3[(k_0 d)^2 - 3 + 3ik_0 d]$. Since $|\mathrm{Im}\{\kappa\}/\mathrm{Re}\{\kappa\}| \ll 1$ and $\mathrm{Re}\{\kappa\} < 0$ for relevant separations $k_0 d \leq 1$, it follows that $\tilde{\alpha} = -i$ is the physically permissible optimum normalized polarizability. Under this condition, radial thermal spin $S_R = +1$ (RCP) when $T_2 \gg T_1$ and $S_R = -1$ (LCP) when $T_2 \ll T_1$ for emission direction $\hat{\mathbf{e}}_R = \hat{\mathbf{e}}_z$ (north pole). At $\hat{\mathbf{e}}_R = -\hat{\mathbf{e}}_z$ (south

pole), the opposite handedness is observed under the same conditions. Figure 2(a) demonstrates this dependence where the two dipoles are assumed to be located at $\mathbf{x}_1 = (0.1, -0.1, 0)1/k_0$ and $\mathbf{x}_2 = (-0.1, 0.1, 0)1/k_0$, having temperatures T_1, T_2. For the top two figures, the vacuum polarizability is $\alpha k_0^3 = 0.22i$ such that the optimum normalized polarizability $\tilde{\alpha} = -i$ is realized. This results in RCP and LCP emission in the northern and southern hemisphere when $T_2 \gg T_1$ and LCP and RCP emission in the northern and southern hemisphere when $T_2 \ll T_1$. This flipping of thermal spin S_R upon inverting the direction follows from the vectorial part of Eq. (8), where the radial spin $S_R \to -S_R$ when $\hat{\mathbf{e}}_R \to -\hat{\mathbf{e}}_R$. As a consequence, the total (integrated over all directions) angular momentum of emitted radiation is zero as expected for a system lacking any intrinsic source of angular momentum. In the context of thermal emission from magneto-optic nanoparticles recently studied in Ref. [19], the cylcotron motion of electrons in the presence of applied magnetic field is responsible for generating angular momentum intrinsically and consequently, the total angular momentum radiated by that particle is nonzero and lies along the direction of applied magnetic field (due to its spherical, isotropic shape).

Dependence on polarizabilities: The top two figures of Fig. 2(a) illustrate the handedness distribution for polarizability $\alpha k_0^3 = 0.22i$, which leads to the normalized polarizability $\tilde{\alpha} = -i$, an optimum design for high-purity CP light along $\pm\hat{\mathbf{e}}_z$ direction. The bottom two figures of Fig. 2(a) illustrate the change in the handedness distribution upon tuning the polarizability to $\alpha k_0^3 = 0.2 + 0.22i$. With this latter configuration, the maximum purity of the radial spin occurs along intermediate and multiple directions indicating that the direction of maximum purity CP emission depends on the polarizabilities and configuration of the antennas. This example shows that the condition $\tilde{\alpha} = \pm i$ obtained above is not a unique and limiting configuration for observing maximum purity CP light from nonequilibrium antennas but other configurations can also be employed. For both these examples, despite complicated directional dependence, northern and southern hemispheres contain the same overall RCP and LCP emission when $T_2 \gg T_1$, with handedness flipped upon $T_2 \leftrightarrow T_1$. Here, we introduce the notation $\leftrightarrow$ to denote the interchange of two quantities in a concise manner. This allows us to summarize the above handedness dependence as RCP $\leftrightarrow$ LCP when $T_2 \leftrightarrow T_1$ or $\hat{\mathbf{e}}_R \leftrightarrow -\hat{\mathbf{e}}_R$ keeping other parameters the same.

Dependence on relative locations of antennas: The overall handedness for northern and southern hemispheres is determined by the relative spatial configuration of dipoles $\hat{\mathbf{e}}_d$, which affects the permissible optimum polarizability ($\tilde{\alpha} = +i$ or $-i$). In particular, for the configuration discussed above, $\hat{\mathbf{e}}_d = (-\hat{\mathbf{e}}_x + \hat{\mathbf{e}}_y)/\sqrt{2}$ leads to $\tilde{\alpha} = -i$ as the physically permissible optimum design along $\pm\hat{\mathbf{e}}_z$. In an alternative configuration with $\hat{\mathbf{e}}_d = (\hat{\mathbf{e}}_x + \hat{\mathbf{e}}_y)/\sqrt{2}$, $\tilde{\alpha} = i$ is the physically permissible value, and this leads to flipping of RCP $\leftrightarrow$ LCP in previous configurations when all other parameters are kept the same. This is illustrated in Fig. 2(b), where L-shaped configuration in the x-y plane with hot vertical and cold horizontal antennas leads to RCP and LCP emission in the northern and southern hemisphere and opposite distribution is observed for its mirror image (in the y-z plane) counterpart.

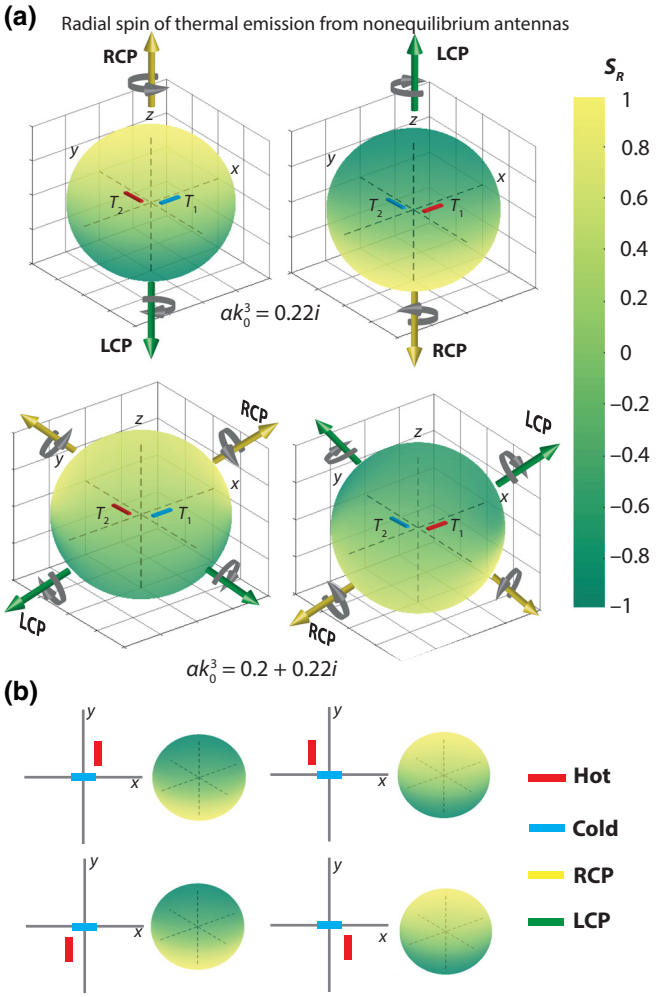

FIG. 2. Radial spin of thermal emission S_R from a dimer of two coupled dipolar antennas is analyzed. Both antennas of dimensionless vacuum polarizability αk_0^3 having temperatures T_1, T_2 and orientations $\hat{\mathbf{e}}_x, \hat{\mathbf{e}}_y$ respectively, are located at $\mathbf{x}_1 = (0.1, -0.1, 0)/k_0$ and $\mathbf{x}_2 = (-0.1, 0.1, 0)/k_0$. (a) Distribution of S_R for two different αk_0^3. The top two figures correspond to optimum design for maximum purity ($S_R = \pm 1$) along $\pm\hat{\mathbf{e}}_z$ directions while the bottom two figures illustrate maximum purity along some intermediate directions for a different value of αk_0^3. The handedness flipping RCP $\leftrightarrow$ LCP is observed upon interchanging temperatures $T_1 \leftrightarrow T_2$ or inverting emission direction $\hat{\mathbf{e}}_R \to -\hat{\mathbf{e}}_R$. (b) Dependence of spin upon the relative spatial orientation of antennas. A mirror image configuration of a given dimer leads to opposite handedness (RCP $\leftrightarrow$ LCP flipping) in the same direction keeping all other parameters the same.

Dependence on orientations of antennas: It further follows from Eq. (8) that RCP $\leftrightarrow$ LCP is expected upon interchanging the dipole orientations ($\hat{\mathbf{e}}_1 \leftrightarrow \hat{\mathbf{e}}_2$), which has an important implication for any isotropic objects. For isotropic objects, the fluctuating dipole moments along all three directions are considered and the radial spin S_R is calculated by considering all dipole pairs. It turns out that the radial spin vanishes for all directions due to spin cancellations from conjugate pairs in the same plane. For instance, S_R emitted by the pair of dipoles $(\tilde{p}_{1x}, \tilde{p}_{2y})$ is always opposite in direction to that emitted by the pair $(\tilde{p}_{1y}, \tilde{p}_{2x})$ due to orientation flipping. Moreover, they are equal in magnitude because $\langle \tilde{p}^*_{1x} \tilde{p}_{2y} \rangle = \langle \tilde{p}^*_{1y} \tilde{p}_{2x} \rangle$, which is true for equal polarizabilities along both directions and provided that the interaction between dipoles is reciprocal. From this, it follows that the anisotropic shape of dipolar objects is necessary to produce CP light. Note that an anisotropic nanoparticle by itself does not emit CP light due to lack of correlations between orthogonal components of its fluctuating dipole moments.

Dependence on distance between antennas: While the dependence of thermal spin on distance d between the dipolar antennas is quite complicated [Eq. (8)], the optimum polarizability condition $\alpha k_0^3 \kappa = \pm i$ provides some useful insights. Since $|\kappa|$ depends inversely on the distance $k_0 d$, it follows that the polarizabilities (αk_0^3) and the separation distance $(k_0 d)$ required for the optimum design are also inversely related. For small distances ($k_0 d \ll 1$), the phase factor $e^{ik_0 d(\hat{\mathbf{e}}_d \cdot \hat{\mathbf{e}}_R)} \sim 1$ in Eq. (8). Under this condition, one can realize maximum purity CP thermal emission with small polarizabilities ($\alpha k_0^3 < 1$) using nonequilibrium antennas discussed above. As we show below, the emission from the antennas at equal temperatures in this regime is at best very weakly polarized. For large separation distances ($k_0 d > 1$) corresponding to negligible near-field interactions, the phase factor $e^{ik_0 d(\hat{\mathbf{e}}_d \cdot \hat{\mathbf{e}}_R)}$ matters and one can numerically optimize the design. However, since $|\kappa| \propto 1/(k_0 d)^3$, the required polarizabilities are very large ($\alpha k_0^3 \gg 1$) and quite difficult to realize with real, practical systems.

Antennas at equal temperatures: For small separation distances $k_0 d \ll 1$, the phase factor $e^{ik_0 d(\hat{\mathbf{e}}_d \cdot \hat{\mathbf{e}}_R)} \sim 1$ simplifies Eq. (8). It then follows that for two antennas of polarizabilities α_1, α_2 having equal temperatures ($T_1 = T_2$), radial spin $S_R \propto \mathrm{Im}\kappa[\mathrm{Im}\alpha_1 \mathrm{Re}\alpha_2 - \mathrm{Im}\alpha_2 \mathrm{Re}\alpha_1]$. Thus, $S_R = 0$ not only for equal vacuum polarizabilities ($\alpha_1 = \alpha_2$) but also when $\alpha_2/\alpha_1 \in \mathbb{R}$ where $\mathbb{R}$ stands for real numbers. Even after overcoming the difficulty of achieving $\alpha_2/\alpha_1 \notin \mathbb{R}$ with engineered design of materials and geometrical shapes, it turns out that, such a dimer produces very weakly polarized radiation. This occurs because of its direct dependence on the dissipative (imaginary) part of near-field coupling ($S_R \propto \mathrm{Im}\{\kappa\}$), which is very small ($\mathrm{Im}\{\kappa\} \ll |\kappa|$) for relevant separations $k_0 d \lesssim 1$. For nonequilibrium antennas discussed above, the thermal spin S_R is non-negligible since it also depends on $\mathrm{Re}\{\kappa\}$ because of unequal temperatures. A dimer of antennas at equal temperatures and having equal (or unequal) polarizabilities always produces unpolarized (or very weakly polarized) thermal radiation.

We note that in order to produce strong CP thermal radiation with antennas at equal temperatures, a many-body system can be considered where the antennas are anisotropic and arranged in a staggered manner so that imaginary-valued correlations between orthogonal dipole moments can be non-negligible through many-body interactions. A metasurface of such anisotropic equilibrium antennas is already explored in Ref. [18], where a kagome lattice of silicon-carbide nanorods is considered. In that work, the resulting emission is predicted to be CP based on the spin-split dispersion of underlying modes achieved with inversion asymmetric metasurface. While the prediction is based on a concrete underlying mechanism, it can be analyzed quantitatively by extending our fluctuational electrodynamic analysis to a many-body system of such dipolar antennas.

Summary of fluctuational electrodynamic analysis: In the following, we point out the important aspects of CP thermal radiation from nonequilibrium coupled antennas by summarizing the dependence of radial spin S_R upon a select few parameters analyzed above:

(a) $S_R \leftrightarrow -S_R$ when $T_1 \leftrightarrow T_2$: The polarization state or handedness of emitted light can be reconfigured by interchanging the temperatures.

(b) $S_R \rightarrow -S_R$ when $\hat{\mathbf{e}}_R \rightarrow -\hat{\mathbf{e}}_R$: Total angular momentum of emitted radiation is zero.

(c) $S_R \leftrightarrow -S_R$ when $\hat{\mathbf{e}}_1 \leftrightarrow \hat{\mathbf{e}}_2$: Cancellation of spin of thermal emission from isotropic dipolar particles. Anisotropic shape is required for generation of CP light.

(d) The maximum purity of CP light from nonequilibrium antennas is $\max\{S_R\} = \pm\Theta(\omega, T_1) - \Theta(\omega, T_2)/\Theta(\omega, T_1) + \Theta(\omega, T_2)$. Its magnitude depends only on the emission wavelength and the antenna temperatures while its direction depends on polarizabilities and geometric configuration of antennas.

Thermal nonequilibrium enables strong CP thermal radiation from a compact dimer of antennas that produces very weakly polarized emission at equilibrium (equal temperatures). Strong CP thermal emission from systems at thermal equilibrium is possible by using optimized chiral absorber metasurfaces [27] or many-body configurations of antennas [18,28]. However, dynamical reconfigurability of circular polarization state with such solid-state designs is a major unsolved problem. Thermal nonequilibrium enables the reconfigurability by simply interchanging the temperatures. Furthermore, reconfigurability can be implemented at arbitrary operating temperatures unlike other potential options of reconfigurability such as phase-change

materials that are limited to certain operating temperatures due to material-specific transition temperatures. Thermal nonequilibrium implemented in a dimer system of antennas can thus achieve three important features of efficient CP-light sources namely, high purity, compactness, and reconfigurability of the polarization state. In the following, we explore the experimental feasibility of this mechanism with suitable practical examples.

III. PRACTICAL IMPLEMENTATION

As a potential experimental system to observe CP thermal emission from nonequilibrium antenna dimers, we consider a system depicted in the insets of Fig. 3 comprising of two arrays of SiC dipolar nanoantennas fabricated on top of suitable microheaters. Silicon carbide is considered a good material choice for studying thermal emission due to large quality factor ($Q \sim 10^3$) phonon-polaritonic resonances, which occur around room-temperature thermal wavelengths ($\lambda \sim 10\ \mu$m). The localized surface polaritonic modes supported by these anisotropic antennas resonantly enhance the polarizabilities (α_1, α_2) as well as the interactions between the antennas. We consider the antennas having length, breadth, and height of 0.4, 0.1, and 0.1 μm, respectively. These can be approximated as prolate ellipsoids [49] having radii $R_a = 200$ nm (major axis) and $R_b = 50$ nm (minor axis). For the realistic examples considered here, the polarizability along the major axis is

$$\alpha(\omega) = \frac{4}{3}\pi R_a R_b^2 \frac{[\varepsilon(\omega) - 1]}{1 + N[\varepsilon(\omega) - 1]}, \tag{9}$$

where N is the geometrical factor dependent on the eccentricity of the ellipsoid $e_c = \sqrt{1 - (R_b/R_a)^2}$ through the following relation [49]:

$$N = \frac{1 - e_c^2}{e_c^2}\left(-1 + \frac{1}{2e_c}\ln\frac{1 + e_c}{1 - e_c}\right),$$

$\varepsilon(\omega)$ is the permittivity of SiC taken from Ref. [50] and is given below:

$$\varepsilon(\omega) = \varepsilon_\infty\left[\frac{\omega^2 - \omega_{\rm LO}^2 + i\Gamma\omega}{\omega^2 - \omega_{\rm TO}^2 + i\Gamma\omega}\right], \tag{10}$$

where $\varepsilon_\infty = 6.7$, $\omega_{\rm LO} = 1.825 \times 10^{14}$ rad/s, $\omega_{\rm TO} = 1.494 \times 10^{14}$ rad/s and $\Gamma = 8.966 \times 10^{11}$ rad/s. The polarizability along minor axis is given by Eq. (9) with the geometrical factor $N' = (1 - N)/2$. It is well known that both polarizabilities are resonantly enhanced (minimization of denominator) at two different frequencies. For the purpose of illustration, we focus on CP thermal emission at frequencies of dipolar resonant modes along major axes. At the corresponding resonant wavelength, the polarizabilities along minor axes are orders of magnitude weak and negligibly affect the dominant thermal emission from polarizabilities along major axes.

The polarizability of these prolate ellipsoids is further influenced by the presence of the substrate. We account for these changes within the dipolar approximation using well-known Green's function technique [37,51]. The modified effective polarizability of the dipolar antennas is $\alpha^{\rm eff}(\omega) = \alpha(\omega)/[1 - \alpha(\omega)k_0^3 G(\omega)]$ where $k_0 = \omega/c$. The expression

$$G(\omega) = \frac{i}{8\pi}\int_0^\infty dk_p \frac{k_p}{\sqrt{1 - k_p^2}}[r^s - (1 - k_p^2)r^p]e^{2i\sqrt{1-k_p^2}d_s} \tag{11}$$

is calculated numerically and it depends on the distance d_s of the antenna dipole from the surface of the metallic heater. r^s, r^p denote the usual Fresnel reflection coefficients for light incident from vacuum onto the substrate. We assume the permittivity of the heater to be $\varepsilon_m = -40 + 10i$ for calculation of Fresnel reflection coefficients. We pick this arbitrary value to reflect the fact that any highly reflective metallic surface such as tungsten, doped semiconductor, metal nitrides can be used in its place. The dependence of the results upon changes in the large negative substrate permittivity is negligible. We note that the dipolar analysis is not accurate for large field gradients and higher-order multipoles contributing when the antennas are separated by small surface-to-surface (antenna surface) separations d_s such that $d_s/R_a < 1$. We avoid this regime for illustration purpose.

Figure 3 describes the thermal emission spin (S_T) along the normal direction ($\hat{\mathbf{e}}_z$) from the dimer pairs. It shows its dependence upon the separation between the antennas **d** and their temperatures, $T_c = 300$ K (cold) and $T_h =$

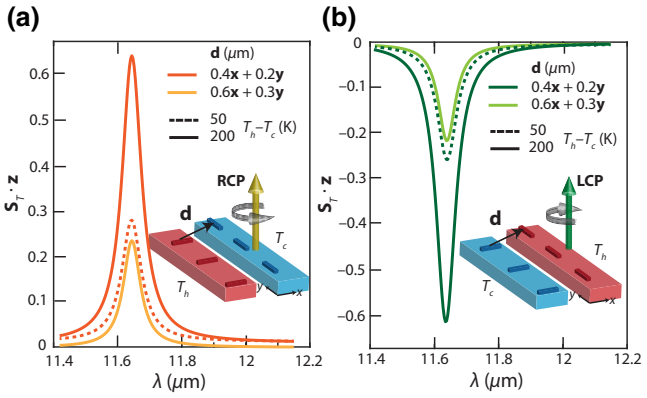

FIG. 3. Two arrays of horizontally and vertically orientated silicon-carbide nanoantennas spatially separated by **d** and fabricated on top of two microheaters maintained at temperatures $T_c = 300$ K (cold) and T_h (hot). Length, breadth, height of each antenna are 0.4, 0.1, 0.1 μm, respectively. (a) When horizontal antennas are at hotter temperature than the vertical antennas, resulting emission is RCP. (b) The handedness of emission is switched to LCP when the temperatures are interchanged.

$T_c + \Delta T$ (hot). We assume that the dimer pairs are separated by distance much larger than **d** and use the arrays to motivate an actual experiment. The magnitude of $S_T \cdot \hat{\mathbf{e}}_z$ for two different separations is shown by light and dark orange (a) and green (b) curves and that for two different ΔT is shown by solid and dashed lines. As depicted in the inset of Fig. 3(a), we first consider a configuration where horizontal dipoles (in x-y plane) are heated to high temperature T_h while the vertical dipoles are maintained at a lower temperature T_c. This results in the emission of RCP light along the normal $\hat{\mathbf{e}}_z$ direction. When the temperatures of the antennas are flipped leading to a configuration depicted in the inset of Fig. 3(b), the resulting emission is LCP keeping all other parameters the same. Since microheater temperatures can be tuned, this enables reconfigurability of the polarization state of the emitted radiation.

As described earlier, for given temperatures T_h and T_c, the maximum purity that can be reached upon design optimization is $[\Theta(\omega, T_h) - \Theta(\omega, T_c)]/[\Theta(\omega, T_h) + \Theta(\omega, T_c)]$ and depends on both wavelength and temperatures. At midinfrared wavelength of 11.6 μm, the proposed device emits strong circularly polarized light with thermal spin $S_T \sim 0.65$ for $\Delta T = 200$ K and $S_T \sim 0.3$ for $\Delta T = 50$ K. Note that the SiC antennas also exchange near-field radiative heat flux of the order of $\lesssim 1$ nW for these configurations (not shown). This near-field heat flux affects the temperatures of antennas. This effect can be monitored in a real experiment and can be analyzed using a separate thermal model. Here, we use reasonable values of steady-state temperatures of the antennas for the calculations. Overall, this analysis of the thermal spin of emission from SiC antenna dimers indicates feasibility of observing reasonably strong CP light under temperature difference of $\Delta T \sim 50$ K across separation of $d \gtrsim 0.5$ μm between the antennas.

One can also consider other Restrahlen materials [52] such as indium phosphide (InP), gallium arsenide (GaAs), indium antimonide (InSb) etc, which support localized polaritons at longer wavelengths and can allow generation of CP light for larger separations. As an example, Fig. 4(a) demonstrates CP-light generation from a dimer of coupled nonequilibrium InP nanoantennas. The permittivity of InP is obtained from Ref. [50] and is described by the Lorentz oscillator model given in Eq. (10) with the following parameters: $\varepsilon_\infty = 9.61$, $\omega_{\mathrm{LO}} = 6.498 \times 10^{13}$ rad/s, $\omega_{\mathrm{TO}} = 5.720 \times 10^{13}$ rad/s and $\Gamma = 6.495 \times 10^{11}$ rad/s. Length, breadth, and height of each antenna are assumed to be 0.8, 0.4, 0.4 μm, respectively. Figure 4(a) shows the spectral thermal spin of emitted radiation when the antennas are separated by a fixed separation of $d \approx 1.1$ μm with temperatures $T_c = 100$ K and T_h (hot). As shown, the thermal emission spin $S_R \sim 0.15$ is obtained for a temperature difference of $\Delta T = 30$ K, indicating the feasibility of observing CP light with smaller ΔT and larger d compared to SiC antennas. This example shows that other

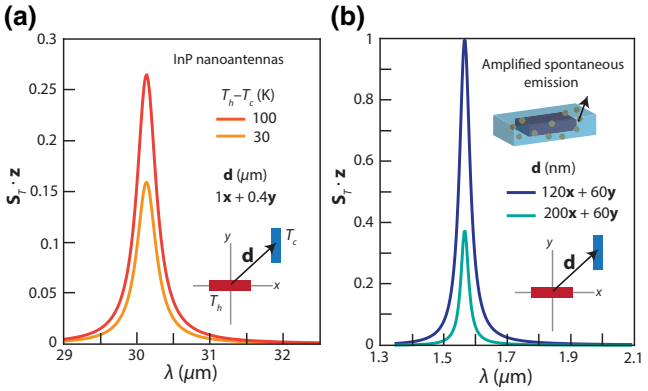

FIG. 4. (a) Thermal emission spin (S_T) for a dimer of InP antennas illustrates feasibility of observing mid-IR CP light with slightly larger gap size for similar $\Delta T = T_h - T_c$, compared to SiC antennas analyzed in Fig. 3. This figure shows that CP-light generation from nonequilibrium antennas is not limited to one particular material choice. Figure (b) demonstrates a conceptual example of a dimer system of antennas where one of the antennas contains gain medium, i.e., a plasmonic antenna enclosed in a dye-doped shell. Well below the lasing threshold, the incoherent amplified spontaneous emission (ASE) from the gain antenna coupled with another nearby antenna can lead to high-purity CP light at suitable separations. This example shows that the proposed mechanism is not limited to "thermal" nonequilibrium but can be potentially implemented in other forms such as population inversion of gain atoms.

materials, operating temperatures, and dimer configurations can be explored to optimize emission of CP light from nonequilibrium antennas.

While we focused so far on thermal nonequilibrium, other forms of nonequilibrium can be potentially implemented using the same dimer configuration. One example is ASE from one of the antennas containing active gain medium where nonequilibrium is in the form of population inversion of gain atoms. The incoherent ASE noise below loss compensation (lasing threshold) is described using fluctuational electrodynamic theory [53,54]. It arises from the fluctuating dipole moments associated with the atomic transitions of gain atoms. These fluctuating sources have an effective temperature dependent on the population inversion and their correlations are described using specific fluctuation-dissipation relations [53,55]. As depicted in the inset of Fig. 4(b), we consider a metallic (e.g., gold, silver) antenna enclosed in a dye-doped shell, which acts as an amplifying medium. Such intricate systems have been considered experimentally in the context of plasmonic nanolasers [56,57]. While large-pump requirements for plasmonic lasing in these geometries make the experimental realization of lasing challenging [58], here we operate with lower gain values (well below lasing threshold) and consider its use for circularly polarized ASE from the dimer.

For this conceptual example, we consider the gain nanoantenna to have an effective permittivity:

$$\varepsilon(\omega) = \underbrace{1 - \frac{\omega_p^2}{\omega_p^2 + i\Gamma\omega_p}}_{\varepsilon_r} + \underbrace{\frac{D_0\gamma_\perp}{(\omega - \omega_{21}) + i\gamma_\perp}}_{\varepsilon_g} \tag{12}$$

consisting of Drude part ε_r and a gain medium part ε_g. The transition frequency of gain atoms is ω_{21} while the strength of (pump-tunable) population inversion is characterized by D_0. We choose the parameters $\omega_p = 4.38 \times 10^{15}$ rad/s, $\Gamma = \omega_p/200$, $\omega_{21} = 1.2 \times 10^{15}$ rad/s, $\gamma_\perp = \omega_{21}/100$. The gain is chosen to be $D_0 = 0.15$ such that $\mathrm{Im}\{\varepsilon\} > 0$ at all wavelengths ensuring ASE regime well below loss compensation. We assume the other nanoantennas to be characterized by the permittivity ε_r. Length, breadth, and height of each antenna are 100, 25, 25 nm, respectively. The polarizabilities $\alpha_{1,2}(\omega)$ are calculated using Eq. (9). The fluctuating dipole moment with ASE from the gain antenna is described by the fluctuation-dissipation relation [55]:

$$\langle p_{1g}^*(\omega) p_{1g}(\omega')\rangle = \frac{2\varepsilon_0}{\omega}\mathrm{Im}\{\alpha_1(\omega)\}\frac{\mathrm{Im}\varepsilon_g(\omega)}{\mathrm{Im}\varepsilon(\omega)}\frac{-n_2\hbar\omega_{21}}{n_2 - n_1}\delta_{\omega,\omega'}, \tag{13}$$

where n_2, n_1 represent the populations in excited and ground states of gain atoms. We assume $n_2 = 0.95n$, $n_1 = n - n_2$ with n as the total number of gain atoms. Since ASE is much larger than the thermal radiation from the antennas, it suffices to calculate the spectral thermal spin of ASE given by Eq. (8) and calculated using above correlations. Figure 4(b) demonstrates the spectral thermal spin for two different separations **d** between the antennas. For the above parameters, the highest purity CP light ($S_R = 1$) is obtained at a wavelength $\lambda = 1.55$ μm, for $d = 134$ nm as shown by the dark blue curve. This conceptual example shows that the proposed mechanism for generating CP light using nonequilibrium antennas is not limited to systems under thermal nonequilibrium. Apart from the use of active gain medium, one can also consider use of biased semiconductors where the heat bath of underlying fluctuating currents has an effective chemical potential or temperature that can be tuned by changing the voltage bias [54,59]. These other forms of nonequilibrium requiring more experimental [56,57] and theoretical details can be explored in separate future works.

Summary of potential experimental platforms: For mid-IR CP thermal emission based on thermal nonequilibrium, one important technical difficulty is that of maintaining large temperature difference across small gaps for high-purity CP light. However, we are confident that the proposed mechanism of CP-light generation can be experimentally implemented in the near future. In particular, there has been a significant experimental progress in the area of near-field radiative heat transfer, which has facilitated exploration of thermal nonequilibrium at nanoscale and has also verified the validity of fluctuational electrodynamic theory [24,25]. In particular, much larger temperature differences ($\Delta T \gtrsim 100$ K) across small gaps $d \lesssim 1$ μm have been experimentally probed in suitable geometries [60,61]. Our analysis of SiC and InP antennas above provides an estimate that reasonably strong CP light ($S_T \sim 0.2$) can be observed with such dimers held at temperature difference as small as $\Delta T \sim 30$ K and separated by a gap size of $d \sim 1$ μm. Such an experiment is fundamentally important as it can reveal the nonintuitive connection between thermal nonequilibrium and angular momentum of light.

In the long run, CP-light emission at near-IR wavelengths and other practical applications such as CP-light-emitting LEDs can be pursued by exploring other nonequilibrium systems considered above. In comparison to other CP-light sources based on structural chirality or polarization conversion, reconfigurability is an important distinct advantage of the proposed mechanism. Related to the tunability of device temperature in the context of CP thermal emission, recent works [36,62,63] have explored dynamical modulation of thermal emission in two-dimensional optoelectronic platforms, where ultrafast switching rates $\gtrsim$100 MHz have been realized. We therefore envision that in the long run, the proposed mechanism can be combined with such newly emerging concepts to build a compact, high-purity, and dynamically reconfigurable source of CP light.

IV. CONCLUSION

We demonstrate a mechanism of CP thermal radiation based on near-field coupling between nonequilibrium antennas. It is unrelated to geometric and material chirality or use of any polarization conversion device. We show that a simple dimer of coupled nonequilibrium antennas can facilitate a great degree of control over the polarization of emitted radiation upon tuning the temperatures, emission direction, relative orientations, and positions of antennas. Through a rigorous fluctuational electrodynamic analysis of the dependence on these parameters, we reveal the fundamental origin and describe the general design guidelines for generating CP light from fluctuating thermal sources. Our analysis revealed that the imaginary-valued correlations between orthogonal components of fluctuating sources are necessary for emission of CP light. In the context of thermal emission from coupled dipolar thermal sources, anisotropic shape is necessary to emit CP thermal radiation. While the computational design with such dipolar bodies is simple and convenient, one can also go beyond this regime with advanced computational tools and inquire about the circular polarization described by

Eq. (6) of thermal emission from arbitrary, nonintuitive geometries [48].

We further explore the experimental feasibility of generating CP light from nonequilibrium antennas with realistic examples of SiC and InP antennas. A reasonably strong CP light from nonequilibrium antennas can be detected in the near future using these example systems. To show that the proposed mechanism is not limited to "thermal" nonequilibrium, we further provide a conceptual example of a plasmonic nanolaser system that can emit circularly polarized amplified spontaneous emission by operating well below lasing threshold. Consideration of such nontrivial approaches is important for practical applications such as CP-light-emitting LEDs.

The underlying approach of analyzing the spin-angular-momentum property of thermal radiation remains largely unexplored in the field of thermal radiation [19]. This approach opens the door to numerous future studies of angular-momentum-related radiative heat-transport phenomena. For instance, one immediate extension of the current work can be consideration of many-body configurations of anisotropic dipolar antennas for shaping angular-momentum properties of light, using thermal nonequilibrium without applying magnetic field. Our analysis also shows a spatial distribution of angular momentum radiated by nonequilibrium antennas. This implies that nontrivial torques on nanoscale bodies can be expected in the vicinity of these antennas. Interestingly, this is already probed by another recent work [35], which demonstrates thermal nonequilibrium enabled torques with temperature-dependent sign and magnitude. This surprising fundamental connection between thermal nonequilibrium and angular momentum of light suggests new possibilities in the context of not only nonequilibrium but also nonisothermal bodies. From the perspective of nanoscale thermometry, detection, and sensing applications, one question that arises is how angular momentum of emitted radiation is influenced by the temperature gradients in nonisothermal bodies, which requires an answer necessarily within fluctuational electrodynamic theory and yet remains unsolved. We leave these inquiries aside for future work.

ACKNOWLEDGMENTS

We thank Ryan Starko-Bowes and Aman Satija for helpful discussions. This work is supported by the U.S. Department of Energy, Office of Basic Energy Science under Award No. DE-SC0017717 and the Lillian Gilbreth Postdoctoral Fellowship program at Purdue University (C.K.).

[1] B. LeFeber, N. Rotenberg, and L. Kuipers, Nanophotonic control of circular dipole emission, Nat. Commun. **6**, 6695 (2015).

[2] R. Mitsch, C. Sayrin, B. Albrecht, P. Schneeweiss, and A. Rauschenbeutel, Quantum state-controlled directional spontaneous emission of photons into a nanophotonic waveguide, Nat. Commun. **5**, 5713 (2014).

[3] I. Žutić, J. Fabian, and S. D. Sarma, Spintronics: Fundamentals and applications, Rev. Mod. Phys. **76**, 323 (2004).

[4] P. Lodahl, S. Mahmoodian, S. Stobbe, A. Rauschenbeutel, P. Schneeweiss, J. Volz, H. Pichler, and P. Zoller, Chiral quantum optics, Nature **541**, 473 (2017).

[5] H. L. Zhu, S. W. Cheung, K. L. Chung, and T. I. Yuk, Linear-to-circular polarization conversion using metasurface, IEEE Trans. Antennas Propag. **61**, 4615 (2013).

[6] C. Pfeiffer, C. Zhang, V. Ray, L. J. Guo, and A. Grbic, High Performance Bianisotropic Metasurfaces: Asymmetric Transmission of Light, Phys. Rev. Lett. **113**, 023902 (2014).

[7] Y. Jiang, L. Wang, J. Wang, C. N. Akwuruoha, and W. Cao, Ultra-wideband high-efficiency reflective linear-to-circular polarization converter based on metasurface at terahertz frequencies, Opt. Express **25**, 27616 (2017).

[8] N. Nishizawa, K. Nishibayashi, and H. Munekata, Pure circular polarization electroluminescence at room temperature with spin-polarized light-emitting diodes, Proc. Natl. Acad. Sci. **114**, 1783 (2017).

[9] P. Asshoff, A. Merz, H. Kalt, and M. Hetterich, A spintronic source of circularly polarized single photons, Appl. Phys. Lett. **98**, 112106 (2011).

[10] D. Di Nuzzo, C. Kulkarni, B. Zhao, E. Smolinsky, F. Tassinari, S. C. J. Meskers, R. Naaman, E. W. Meijer, and R. H. Friend, High circular polarization of electroluminescence achieved via self-assembly of a light-emitting chiral conjugated polymer into multidomain cholesteric films, ACS Nano **11**, 12713 (2017).

[11] D. Zhao, H. He, X. Gu, L. Guo, K. S. Wong, J. W. Y. Lam, and B. Z. Tang, Circularly polarized luminescence and a reflective photoluminescent chiral nematic liquid crystal display based on an aggregation-induced emission luminogen, Adv. Opt. Mater. **4**, 534 (2016).

[12] Y. J. Zhang, T. Oka, R. Suzuki, J. T. Ye, and Y. Iwasa, Electrically switchable chiral light-emitting transistor, Science **344**, 725 (2014).

[13] J. Kumar, T. Nakashima, and T. Kawai, Circularly polarized luminescence in chiral molecules and supramolecular assemblies, J. Phys. Chem. Lett. **6**, 3445 (2015).

[14] E. M. Sánchez-Carnerero, A. R. Agarrabeitia, F. Moreno, B. L. Maroto, G. Muller, M. J. Ortiz, and S. de la Moya, Circularly polarized luminescence from simple organic molecules, Chem.: Eur. J. **21**, 13488 (2015).

[15] K. Konishi, M. Nomura, N. Kumagai, S. Iwamoto, Y. Arakawa, and M. Kuwata-Gonokami, Circularly Polarized Light Emission From Semiconductor Planar Chiral Nanostructures, Phys. Rev. Lett. **106**, 057402 (2011).

[16] A. A. Maksimov, I. I. Tartakovskii, E. V. Filatov, S. V. Lobanov, N. A. Gippius, S. G. Tikhodeev, C. Schneider, M. Kamp, S. Maier, S. Höfling, and V. D. Kulakovskii, Circularly polarized light emission from chiral spatially-structured planar semiconductor microcavities, Phys. Rev. B **89**, 045316 (2014).

[17] S. L. Wadsworth, P. G. Clem, E. D. Branson, and G. D. Boreman, Broadband circularly-polarized infrared

emission from multilayer metamaterials, Opt. Mater. Express **1**, 466 (2011).
[18] N. Shitrit, I. Yulevich, E. Maguid, D. Ozeri, D. Veksler, V. Kleiner, and E. Hasman, Spin-optical metamaterial route to spin-controlled photonics, Science **340**, 724 (2013).
[19] A. Ott, P. Ben-Abdallah, and S. A. Biehs, Circular heat and momentum flux radiated by magneto-optical nanoparticles, Phys. Rev. B **97**, 205414 (2018).
[20] S. M. Rytov, Theory of electric fluctuations and thermal radiation, AFCRC-TR **59**, 162 (1959).
[21] L. D. Landau and E. M. Lifshitz, *Course of Theoretical Physics* (Butterworth-Heinemann, Oxford, 1980), Vol. 5, **3**.
[22] S. M. Barnett, L. Allen, and M. J. Padgett, *Optical Angular Momentum* (CRC Press, Boca Raton, 2016).
[23] L. Allen, M. W. Beijersbergen, R. J. C. Spreeuw, and J. P. Woerdman, Orbital angular momentum of light and the transformation of Laguerre-Gaussian laser modes, Phys. Rev. A **45**, 8185 (1992).
[24] B. Song, A. Fiorino, E. Meyhofer, and P. Reddy, Near-field radiative thermal transport: From theory to experiment, AIP Adv. **5**, 053503 (2015).
[25] K. Kim, B. Song, V. Fernández-Hurtado, W. Lee, W. Jeong, L. Cui, D. Thompson, J. Feist, M. T. H. Reid, F. J. García-Vidal, J. C. Cuevas, E. Meyhofer, and P. Reddy, Radiative heat transfer in the extreme near field, Nature **528**, 387 (2015).
[26] E. Tervo, E. Bagherisereshki, and Z. Zhang, Near-field radiative thermoelectric energy converters: A review, Front. Energy **12**, 5 (2018).
[27] C. Wu, N. Arju, G. Kelp, J. A. Fan, J. Dominguez, E. Gonzales, E. Tutuc, I. Brener, and G. Shvets, Spectrally selective chiral silicon metasurfaces based on infrared fano resonances, Nat. Commun. **5**, 3892 (2014).
[28] X. Yin, M. Schaferling, B. Metzger, and H. Giessen, Interpreting chiral nanophotonic spectra: The plasmonic Born–Kuhn model, Nano Lett. **13**, 6238 (2013).
[29] K. Y. Bliokh, A. Y. Bekshaev, and F. Nori, Optical Momentum, Spin, and Angular Momentum in Dispersive Media, Phys. Rev. Lett. **119**, 073901 (2017).
[30] K. Y. Bliokh, A. Y Bekshaev, and F. Nori, Dual electromagnetism: Helicity, spin, momentum and angular momentum, New J. Phys. **15**, 033026 (2013).
[31] T. Van Mechelen and Z. Jacob, Universal spin-momentum locking of evanescent waves, Optica **3**, 118 (2016).
[32] E. Moncada-Villa, V. Fernández-Hurtado, F. J. Garcia-Vidal, A. García-Martín, and J. C. Cuevas, Magnetic field control of near-field radiative heat transfer and the realization of highly tunable hyperbolic thermal emitters, Phys. Rev. B **92**, 125418 (2015).
[33] W. Jin, A. G. Polimeridis, and A. W. Rodriguez, Temperature control of thermal radiation from composite bodies, Phys. Rev. B **93**, 121403(R) (2016).
[34] S. E. Han and D. J. Norris, Control of Thermal Emission by Selective Heating of Periodic Structures, Phys. Rev. Lett. **104**, 043901 (2010).
[35] M. T. H. Reid, O. D. Miller, A. G. Polimeridis, A. W. Rodriguez, E. M. Tomlinson, and S. G. Johnson, Photon torpedoes and rytov pinwheels: Integral-equation modeling of non-equilibrium fluctuation-induced forces and torques on nanoparticles, arXiv:1708.01985 (2017).
[36] E. Sakat, L. Wojszvzyk, J. P. Hugonin, M. Besbes, C. Sauvan, and J. Greffet, Enhancing thermal radiation with nanoantennas to create infrared sources with high modulation rates, Optica **5**, 175 (2018).
[37] L. Novotny and B. Hecht, *Principles of Nano-Optics* (Cambridge University Press, Cambridge, England, 2012).
[38] P. Ben-Abdallah, S. A. Biehs, and K. Joulain, Many-Body Radiative Heat Transfer Theory, Phys. Rev. Lett. **107**, 114301 (2011).
[39] G. Domingues, S. Volz, K. Joulain, and J. Greffet, Heat Transfer Between Two Nanoparticles Through Near Field Interaction, Phys. Rev. Lett. **94**, 085901 (2005).
[40] K. Joulain, J. Mulet, F. Marquier, R. Carminati, and J. Greffet, Surface electromagnetic waves thermally excited: Radiative heat transfer, coherence properties and casimir forces revisited in the near field, Surf. Sci. Rep. **57**, 59 (2005).
[41] M. V. Berry, Paraxial beams of spinning light, Int. Conf. Singular Optics **3487**, 6 (1998).
[42] T. Setälä, M. Kaivola, and A. T. Friberg, Degree of Polarization in Near Fields of Thermal Sources: Effects of Surface Waves, Phys. Rev. Lett. **88**, 123902 (2002).
[43] O. V. Angelsky, A. Y. Bekshaev, P. P. Maksimyak, A. P. Maksimyak, I. I. Mokhun, S. G. Hanson, C. Y. Zenkova, and A. V. Tyurin, Circular motion of particles suspended in a Gaussian beam with circular polarization validates the spin part of the internal energy flow, Opt. Express **20**, 11351 (2012).
[44] A. Canaguier-Durand, A. Cuche, C. Genet, and T. W. Ebbesen, Force and torque on an electric dipole by spinning light fields, Phys. Rev. A **88**, 033831 (2013).
[45] M. Nieto-Vesperinas, Optical torque: Electromagnetic spin and orbital-angular-momentum conservation laws and their significance, Phys. Rev. A **92**, 043843 (2015).
[46] S. Edalatpour and M. Francoeur, The thermal discrete dipole approximation (t-dda) for near-field radiative heat transfer simulations in three-dimensional arbitrary geometries, J. Quant. Spectrosc. Radiat. Transf. **133**, 364 (2014).
[47] S. Edalatpour, M. Čuma, T. Trueax, R. Backman, and M. Francoeur, Convergence analysis of the thermal discrete dipole approximation, Phys. Rev. E **91**, 063307 (2015).
[48] M. T. Homer Reid and Steven G. Johnson, Efficient computation of power, force, and torque in beam scattering calculations, IEEE Trans. Antennas Propag. **63**, 3588 (2015).
[49] C. F. Bohren and D. R. Huffman, *Absorption and Scattering of Light by Small Particles* (John Wiley & Sons, Weinheim, 2008).
[50] E. D. Palik, *Handbook of Optical Constants of Solids* (Academic Press, Cambridge, Massachusetts, 1998), Vol. 3.
[51] B. Amorim, P. A. D. Gonçalves, M. I. Vasilevskiy, and N. M. R. Peres, Impact of graphene on the polarizability of a neighbour nanoparticle: A dyadic Green's function study, Appl. Sci. **7**, 1158 (2017).
[52] J. D. Caldwell, L. Lindsay, V. Giannini, I. Vurgaftman, T. L. Reinecke, S. A. Maier, and O. J. Glembocki, Low-loss, infrared and terahertz nanophotonics using surface phonon polaritons, Nanophotonics **4**, 44 (2015).
[53] R. Matloob, R. Loudon, M. Artoni, S. M. Barnett, and J. Jeffers, Electromagnetic field quantization in amplifying dielectrics, Phys. Rev. A **55**, 1623 (1997).

[54] C. H. Henry and R. F. Kazarinov, Quantum noise in photonics, Rev. Mod. Phys. **68**, 801 (1996).
[55] C. Khandekar, W. Jin, O. D. Miller, A. Pick, and A. W. Rodriguez, Giant frequency-selective near-field energy transfer in active–passive structures, Phys. Rev. B **94**, 115402 (2016).
[56] M. A. Noginov, G. Zhu, A. M. Belgrave, R. Bakker, V. M. Shalaev, E. E. Narimanov, S. Stout, E. Herz, T. Suteewong, and U. Wiesner, Demonstration of a spaser-based nanolaser, Nature **460**, 1110 (2009).
[57] K. G. Stamplecoskie, M. Grenier, and J. C. Scaiano, Self-assembled dipole nanolasers, J. Am. Chem. Soc. **136**, 2956 (2014).
[58] M. Premaratne and M. I. Stockman, Theory and technology of spasers, Adv. Opt. Photonics **9**, 79 (2017).
[59] K. Chen, P. Santhanam, S. Sandhu, L. Zhu, and S. Fan, Heat-flux control and solid-state cooling by regulating chemical potential of photons in near-field electromagnetic heat transfer, Phys. Rev. B **91**, 134301 (2015).
[60] M. P. Bernardi, D. Milovich, and M. Francoeur, Radiative heat transfer exceeding the blackbody limit between macroscale planar surfaces separated by a nanosize vacuum gap, Nat. Commun. **7**, 12900 (2016).
[61] M. Ghashami, H. Geng, T. Kim, N. Iacopino, S. K. Cho, and K. Park, Precision Measurement of Phonon-Polaritonic Near-Field Energy Transfer Between Macroscale Planar Structures Under Large Thermal Gradients, Phys. Rev. Lett. **120**, 175901 (2018).
[62] T. Mori, Y. Yamauchi, S. Honda, and H. Maki, An electrically driven, ultrahigh-speed, on-chip light emitter based on carbon nanotubes, Nano Lett. **14**, 3277 (2014).
[63] Y. D. Kim *et al.*, Ultrafast graphene light emitters, Nano Lett. **18**, 934 (2018).